Structural Engineering and Mechanics, Vol. 24, No. 6 (2006) 665-682
DOI: http://dx.doi.org/10.12989/sem.2006.24.6.665

Nondestructive damage evaluation of a curved thin beam

Byeong Hwa Kim†

Research Institute of Industrial Science & Technology, Steel Structure Research Lab, 79-5 Yeongcheon, Dongtan, Hwaseong, Gyeonggi 445-813, Korea

Hwan Joong Joo‡ and Taehyo Park‡†

Department of Civil Engineering, Hanyang University, 17 Haengdang-dong, Seoul 133-791, Korea

(Received September 9, 2004, Accepted August 1, 2006)

Abstract. A vibration-based nondestructive damage evaluation technique for a curved thin beam is introduced. The proposed method is capable of detecting, locating, and sizing structural damage simultaneously by using a few of the lower natural frequencies and their corresponding mode shapes before and after a small damage event. The proposed approach utilizes modal flexibilities reconstructed from measured modal parameters. A rigorous system of equations governing damage and curvature of modal flexibility is derived in the context of elasticity. To solve the resulting system of governing equations, an efficient *pseudo*-inverse technique is introduced. The direct inspection of the resulting solutions provides the location and severity of damage in a curved thin beam. This study confirms that there is a strong linear relationship between the curvature of modal flexibility and flexural damage in the selected class of structures. Several numerical case studies are provided to justify the performance of the proposed approach. The proposed method introduces a way to avoid the singularity and mode selection problems from earlier attempts.

Keywords: damage detection; flexural damage index; curvature of mode shape; modal flexibility; curved thin beam; circular arch.

1. Introduction

Structures are often exposed to unexpected hostile environments that may cause structural damage. Since the accumulation of structural damage may result in catastrophic failure, the periodic inspection of the load carrying capacity of a structure is a necessity. To periodically monitor the integrity of structures, a nondestructive, non-intrusive, and inexpensive damage evaluation technique is necessary. Vibration-based Nondestructive Damage Evaluation (NDE) methods draw special attention for such applications.

The vibration-based NDE method has evolved over the last two decades, and is based on the concept that changes in local stiffness are reflected by changes in eigenvalues (Cawley and Adams

† Research Associate
‡ Graduate Student
‡†Associate Professor, Corresponding author, E-mail: cepark@hanyang.ac.kr

1979). The promising features of the sensitivity-based frequency approach proposed by Stubbs (1985) are as follows: (1) few measurement points are required, since frequency information is independent of the probing position; (2) low input energy levels are sufficient to produce measurable responses (Salawu 1997); (3) a frequency shift has less statistical variation than other modal parameters (Mottershead and Friswell 1993); (4) the method can be implemented to structural health monitoring because the resonance frequencies can easily be extracted from ambient vibration responses induced by normal traffic or winds. However, there are also some drawbacks to the frequency approach. For instance, the site's air temperature, humidity, mean air pressure, and mean rainfall on the day preceding the test may affect resonant frequencies (Farrar *et al.* 2000). Also, the changes in natural frequency caused by damage at two symmetric locations in symmetric structures are exactly the same. Furthermore, an inverse problem arises if the number of measurable frequencies is less than the number of unknown damaged locations.

Related to the drawbacks of earlier attempts, the utilization of mode shapes in the vibration-based NDE method is fairly common. The Mode Shape Curvature (MSC) method proposed by Pandey *et al.* (1999) reveals that the amount of damage in a structure can be obtained from the magnitude of changes in mode shape curvature before and after damage. In their numerical studies, the changes in resonant frequencies, modal assurance criterion, and displacement mode shapes did not indicate the presence of damage. Only changes in mode shape curvature indicated the location of damage. Still, the MSC method has the following shortcomings: (1) the singularity problems near the inflection points of mode shapes is an obstacle to damage detection (Chen and Swamidas 1994); (2) the estimated results can be different if more than one mode is used (Doebling *et al.* 1996); (3) the method requires a sufficient restricted spatial resolution of sensors (Chen and Swamidas 1994); (4) the method cannot predict such damage as a uniform reduction in global stiffness (Salawu and Williams 1994); (5) the method is not valid for axial modes because the method is based on the flexural formula of an Euler-Bernoulli beam. Among the difficulties presented, the third, fourth, and fifth shortcomings are considered to be minor obstacles to damage detection for the following reasons: (1) a few of the lower flexural modes, instead of the relatively higher axial modes, are most important in practice, (2) the most probable location of damage is the place that maximum deflection occurs, and (3) high resolution in sensor locations is achievable but costly. The major difficulties of the MSC method lie in the singularity and mode selection problems. Wahab and Roeck (1999) attempted to resolve the mode selection problems by proposing a curvature damage factor, or an arithmetic mean of changes in the mode shape curvature for all modes. However, the absolute severity of damage relative to an intact structure could not be achieved due to the lack of a physical interpretation of the proposed factor.

The Damage Index (DI) method proposed by Stubbs *et al.* (1995) can be considered as another notable effort to localize damage using mode shapes. The underlying assumption of the DI method is that the sensitivity of factional modal strain energy of a potential damaged element is invariant before and after a small damage event. The element-wise factional modal strain energy is approximated by the numerical integration of curvature mode shapes. A *Spline* interpolation between two sensor locations is a prerequisite to achieving a good curvature profile of measured mode shapes with typically coarse sensor intervals. Such an interpolation step is not a component of the MSC method. The DI method was originally developed for an Euler-Bernoulli beam and was later specialized for plates (Choi and Stubbs 1997, Cornwell *et al.* 1999) and cylindrical shells (Srinivasan and Kot 1998). Although it seems that the DI method is more refined than the MSC method, the DI method suffers from the same difficulties as the MSC method. Consequently, the DI

method cannot estimate the absolute severity of damage, even if the localization of damage is distinguishable from other methods (Farrar and Jauregui 1998, Ndambi *et al.* 2002).

Since both the DI and the MSC methods directly identify damage from response signatures without involving any numerical model modification step such as a sensitivity updating algorithm, they are fast, inexpensive, and non-intrusive. However, the accuracy of measured mode shapes relies not only on sampling frequency but also on magnitude resolution of frequency response function. Thus, the cautious selection of sensitivity of sensors to the expected range of vibration magnitude is necessary. Furthermore, the second order derivatives of measured mode shapes are required, because a feature common to the MSC and DI methods is the utilization of mode shape curvature. Clearly, unexpected measurement noise could be involved in this step. However, this situation could be avoided either by conducting the sufficient number of modal testing and analysis, or by using the state-of-the-art laser sensing technology. In any case, the small variances and standard deviations on measured mode shapes should be confirmed before applying the deterministic mode shape based damage detection methods.

Based on the common feature of the MSC and DI methods, it is natural to deduce a strong relationship between curvature and damage. However, the existing MSC and DI methods fail to estimate the absolute severity of damage. The major obstacles to damage severity estimation may be the mode selection and singularity problems. This study introduces an attempt to resolve the aforementioned deficiencies of the DI and MSC methods for a selected class of structures. The approach introduced uses modal flexibility to avoid the mode selection problem. A commonly accepted feature of modal flexibility, related to damage detection, is the fact that modal flexibility can accurately be estimated by a few of the lower modes. In the case of damage detection, modal flexibility can be considered to be a rational way to combine modes. Consequently, a single representative solution can be achieved. To resolve the singularity problem, a set of coupled equations that represent a damage mechanism near the singularity points is sought and solved. To achieve the objective with those strategies, the following four steps are conducted. First, the slope-deflection formula for a curved beam is derived after introducing the background of modal flexibility. Second, a damage mechanism of a curved element is unveiled using the finite difference approach. Third, an efficient solution procedure to solve a derived equation governing the damage mechanism is discussed. Finally, a set of numerical verifications is provided to examine the performance of the proposed method.

2. A theory of damage detection

2.1 The jth modal flexibility

The flexibility matrix is known as the inversion of the global stiffness matrix of a structure. The jth column in the flexibility matrix represents a deflection profile caused by a unit load at the jth degree of freedom (DOF). In the following discussion, the jth modal flexibility vector is defined as the modal approximation of the jth column of the flexibility matrix. The jth modal flexibility vector, denoted by $\mathbf{w}_j$, can be obtained as follows (Berman and Flannelly 1971);

$$\mathbf{w}_j = \sum_{i=1}^{r} \frac{\varphi_{ji}}{\lambda_i m_i} \boldsymbol{\varphi}_i \tag{1}$$

where $\boldsymbol{\varphi}_i$ denotes the ith displacement normalized mode shape vector; φ_{ji} denotes the jth scalar components of $\boldsymbol{\varphi}_i$; λ_i denotes the ith eigenvalue; m_i denotes the ith modal mass; and the upper limit, r, denotes the number of measured modes. If the mass normalized mode shape is available, the jth modal flexibility vector can be expressed by

$$\mathbf{w}_j = \sum_{i=1}^{r} \frac{\psi_{ji}}{\lambda_i} \boldsymbol{\psi}_i \tag{2}$$

where $\boldsymbol{\psi}_i = \boldsymbol{\varphi}_i / \sqrt{m_i}$ denotes the ith mass normalized mode shape (Ewin 2000) and ψ_{ji} denotes the jth component of $\boldsymbol{\psi}_i$. Note that the jth modal flexibility vector accurately approximates the static deflection due to a unit load by utilizing only a few of the lower modes. The reason is that the ith modal contribution factor (ψ_{ji}/λ_i or $\varphi_{ji}/m_i\lambda_i$) rapidly decreases as the frequency increases. Furthermore, the kth component of $\mathbf{w}_j$ represents the displacement at the kth node caused by an applied unit load at the jth DOF.

$$w_{kj} = \sum_{i=1}^{r} \frac{\psi_{ji}\psi_{ki}}{\lambda_i} = w_{jk} \tag{3}$$

Since $w_{kj} = w_{jk}$, the reciprocal theorem is still valid even if the jth or kth modal flexibility vector is truncated. It is interesting that the deflection at an arbitrary position caused by applied loads can be achieved by knowing the eigenvalues and eigenvectors without any knowledge of the material properties of a system.

The input and the output responses of a structure are available in the forced vibration tests. Consequently, mass normalized mode shapes can be easily determined by existing modal analysis techniques and the jth modal flexibility vector can be synthesized using Eq. (2). However, in the case of ambient vibration tests, mass normalized mode shapes cannot be determined because the input is unknown. In such a case, the ith modal mass can be approximated by the numerical integration of the following formula:

$$m_i = \int_0^L \rho A \, \varphi_i(s) \, \varphi_i(s) ds \tag{4}$$

where the function $\varphi_i(s)$ denotes the ith displacement normalized mode shape. To approximate the ith modal mass, a *cubic Spline* interpolation of the mode shapes is recommended prior to numerical integration. Using the estimated modal mass and the displacement normalized mode shapes, the jth modal flexibility vector can be obtained by Eq. (1).

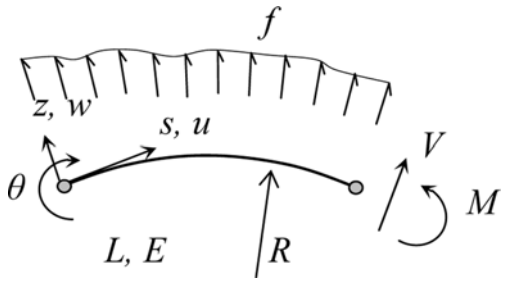

Fig. 1 Sign convention of a curved beam

2.2 Slope deflection equation for a curved thin beam

A slope-deflection equation for a curved thin beam is derived in this section. Consider the curved thin beam element with a radius of R shown in Fig. 1. The symbols s and z denote the tangential and radial coordinates, respectively. The symbols u and w denote the tangential and radial deflections caused by distributed load f, respectively. Tangential strain, ε_s, at an arbitrary point (s, z) can be expressed as

$$\varepsilon_s = \varepsilon_m - z\chi \tag{5}$$

in which

$$\varepsilon_m = \frac{\partial u}{\partial s} + \frac{w}{R} \quad \text{and} \quad \chi = -\frac{1}{R}\frac{\partial u}{\partial s} + \frac{\partial^2 w}{\partial s^2} \tag{6}$$

where ε_m denotes membrane strain along the midline of the curved beam and χ denotes curvature change associated with bending moment M. Here, curvature change is considered positive when the radius of curvature decreases. Under most loading conditions, the displacements caused by the extension of the centerline of a slender arch or thin ring are very small in comparison with the displacements caused by bending (Timoshenko and Gere 1963). At the limit of slenderness, inextensibility assumption $\varepsilon_m = 0$ implies

$$\frac{\partial u}{\partial s} = -\frac{w}{R} \tag{7}$$

Combining Eq. (6) and Eq. (7) with Eq. (5) yields the inextensible strain-displacement relationship:

$$\varepsilon_s = -z\left(\frac{w}{R^2} + \frac{\partial^2 w}{\partial s^2}\right) \tag{8}$$

The virtual work done by a normal stress fiber caused by virtual strain $\delta\varepsilon_s$ can be described as

$$\delta W_0 = \sigma_s \delta\varepsilon_s \tag{9}$$

where δ denotes the variational operator and σ_s denotes normal stress in the tangential direction. Assuming that the material follows Hook's law, $\sigma_s = E\varepsilon_s$, the virtual work done by a normal stress fiber is given by

$$\delta W_0 = Ez^2\left(\frac{w}{R^2} + \frac{\partial^2 w}{\partial s^2}\right)\left(\frac{\delta w}{R^2} + \frac{\partial^2 \delta w}{\partial s^2}\right) \tag{10}$$

where E denotes the modulus of elasticity. Then, the internal virtual work done, δW_I, by a body owing to the elastic deformation is given by integrating δW_0 with respect to the volume:

$$\delta W_I = \int_V \delta W_0 dV \tag{11}$$

The external virtual work done δW_E, owing to the distributed surface radial loads f, can be described as

$$\delta W_E = -\int_0^L f \delta w \, ds \tag{12}$$

The negative sign implies that work is performed on the body. With the aid of a double integration by the parts, the total virtual work done, $\delta W = \delta W_I + \delta W_E$, can be expressed by

$$\delta W = \int_0^L \left[\frac{\partial^2}{\partial s^2}\left(EI \frac{\partial^2 w}{\partial s^2} \right) + \frac{EI}{R^2}\frac{\partial^2 w}{\partial s^2} + \frac{\partial^2}{\partial s^2}\left(\frac{EI}{R^2} w \right) + \frac{EI}{R^4} w - f \right] \delta w \, ds$$
$$- \frac{\partial}{\partial s}\left[EI\left(\frac{w}{R^2} + \frac{\partial^2 w}{\partial s^2} \right) \right] \delta w \Big|_0^L - EI\left(\frac{w}{R^2} + \frac{\partial^2 w}{\partial s^2} \right) \delta\left(\frac{\partial w}{\partial s} \right) \Big|_0^L \tag{13}$$

The principle of virtual displacement, $\delta W = 0$, gives rise to the equilibrium equation as well as to the boundary conditions on the forces (i.e., ending moments M and shear force V):

$$\frac{\partial^2}{\partial s^2}\left(EI \frac{\partial^2 w}{\partial s^2} \right) + \frac{EI}{R^2}\frac{\partial^2 w}{\partial s^2} + \frac{\partial^2}{\partial s^2}\left(\frac{EI}{R^2} w \right) + \frac{EI}{R^4} w = f \quad \text{for} \quad 0 < s < L \tag{14}$$

$$M = EI\left(\frac{w}{R^2} + \frac{\partial^2 w}{\partial s^2} \right) \quad \text{at} \quad s = 0 \text{ and } L \tag{15}$$

$$V = \frac{\partial M}{\partial s} \quad \text{at} \quad s = 0 \text{ and } L \tag{16}$$

Note that the above governing equation and force equations are similar to those of the Euler-Bernoulli beam when the radius R approaches infinity.

Consider a circular arch, as depicted in Fig. 2(a), with a uniform cross section and a radius R. The arch is subjected to a unit load at the jth node. Suppose that the static radial deflection profile of the curved beam is accurately approximated at the sensor locations by the jth modal flexibility vector, $\mathbf{w}_j$, using Eq. (1) or Eq. (2). Then the governing equation of the eth circular beam element, as shown in Fig. 2(b), can be achieved using Eq. (14):

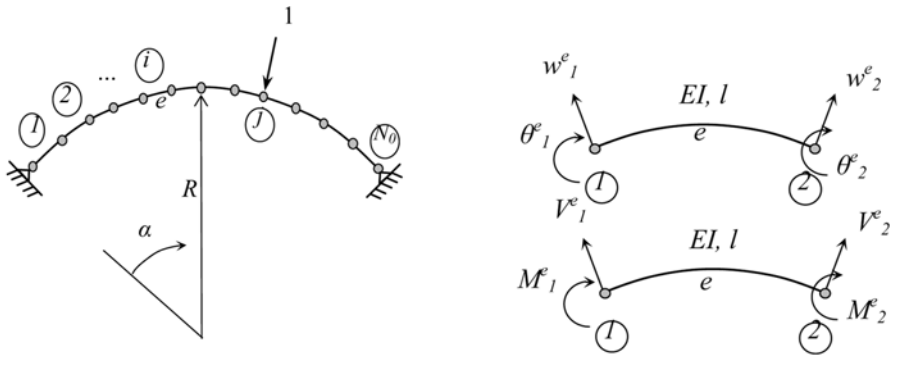

(a) The jth modal flexibility (b) Local coordinates of the eth element

Fig. 2 The jth modal flexibility of a circular arch

$$\frac{d^4w}{ds^4} + \frac{2}{R^2}\frac{d^2w}{ds^2} + \frac{w}{R^4} = 0 \tag{17}$$

Note that the eth element has a constant flexural rigidity EI, a constant radius R, and an arc length l. In addition, no radial distributed surface load f is applied. For this homogeneous fourth order ordinary differential equation, the roots of the characteristic equation, $(\eta^2+1)^2 = 0$, are $\eta = \{i, i, -i, -i\}$. The exact solution has the following form:

$$w(s) = \alpha_1 \sin\left(\frac{s}{R}\right) + \alpha_2 \cos\left(\frac{s}{R}\right) + \alpha_3 \frac{s}{R}\sin\left(\frac{s}{R}\right) + \alpha_4 \frac{s}{R}\cos\left(\frac{s}{R}\right) \tag{18}$$

where α_i is an arbitrary constant that depends on the specific boundary conditions. Eq. (18) can be rewritten as

$$w(s) = \mathbf{p}^T(s)\boldsymbol{\alpha} \tag{19}$$

in which

$$\mathbf{p}(s) = \left[\sin\left(\frac{s}{R}\right) \quad \cos\left(\frac{s}{R}\right) \quad \frac{s}{R}\sin\left(\frac{s}{R}\right) \quad \frac{s}{R}\cos\left(\frac{s}{R}\right)\right]^T \tag{20}$$

and

$$\boldsymbol{\alpha} = [\alpha_1 \quad \alpha_2 \quad \alpha_3 \quad \alpha_4]^T \tag{21}$$

To obtain the four unknowns, denoted as α_i, four boundary conditions are required. Since the primary variables in Eq. (13) are w and $\partial w/\partial s$, they must be specified at two ends of the element. Such essential boundary conditions of the eth element are as follows:

$$w(0) \equiv w_1^e, \quad \theta(0) \equiv \theta_1^e, \quad w(l) \equiv w_2^e, \quad \theta(l) \equiv \theta_2^e \tag{22}$$

where, $\theta(s) = -dw(s)/ds$ denotes the rotational DOF, and l denotes the length of the eth element considered. Combining Eq. (19) with Eq. (22) yields the equation:

$$\begin{bmatrix} w_1^e \\ \theta_1^e \\ w_2^e \\ \theta_2^e \end{bmatrix} = \begin{bmatrix} 0 & 1 & 0 & 0 \\ -\frac{l}{R} & 0 & 0 & -\frac{l}{R} \\ \sin\left(\frac{l}{R}\right) & \cos\left(\frac{l}{R}\right) & \frac{l}{R}\sin\left(\frac{l}{R}\right) & \frac{l}{R}\cos\left(\frac{l}{R}\right) \\ -\frac{1}{R}\cos\left(\frac{l}{R}\right) & \frac{1}{R}\sin\left(\frac{l}{R}\right) & -\frac{1}{R^2}\cos\left(\frac{l}{R}\right) - \frac{1}{R}\sin\left(\frac{l}{R}\right) & -\frac{1}{R}\cos\left(\frac{l}{R}\right) + \frac{1}{R^2}\sin\left(\frac{l}{R}\right) \end{bmatrix} \begin{bmatrix} \alpha_1 \\ \alpha_2 \\ \alpha_3 \\ \alpha_4 \end{bmatrix} \tag{23}$$

In a matrix form, Eq. (23) can be rewritten as:

$$\mathbf{w}^e = \mathbf{C}\boldsymbol{\alpha} \tag{24}$$

where the 4×1 vector $\mathbf{w}^e = [w_1^e \ \theta_1^e \ w_2^e \ \theta_2^e]^T$ denotes a set of the primary nodal variables. Inverting the matrix, $\mathbf{C}$, the coefficient vector, α, can be directly obtained.

$$\alpha = \mathbf{C}^{-1}\mathbf{w}^e \tag{25}$$

Substituting Eq. (25) into Eq. (19) yields the radial deflection, $w(s)$, in terms of the primary nodal variables:

$$w(s) = \mathbf{N}^T(s)\mathbf{w}^e \tag{26}$$

where the 4×1 vector $\mathbf{N}(s) = \mathbf{C}^{-T}\mathbf{p}(s)$ is called an interpolation matrix.

Substituting the radial deflection in terms of the primary nodal variables in Eq. (26) into Eq. (15) yields:

$$M(s) = EI\mathbf{B}(s)^T\mathbf{w}^e \tag{27}$$

where the 4×1 vector, $\mathbf{B}(s) = \mathbf{N}(s)/R^2 + d^2\mathbf{N}(s)/ds^2$, denotes the curvature of the element. Thus, the internal moments at any point along the beam element can be estimated if all the primary nodal variables can be measured. Substituting $s = 0$ and $s = l$ in Eq. (27) yields the internal moments, M_1^e and M_2^e, at the two end nodes in terms of the primary nodal variables, respectively.

$$\begin{bmatrix} M_1^e \\ M_2^e \end{bmatrix} = \begin{bmatrix} c_1\dfrac{EI_1^e}{l} & c_2\dfrac{EI_2^e}{l} \\ -c_2\dfrac{EI_1^e}{l} & -c_1\dfrac{EI_2^e}{l} \end{bmatrix} \begin{bmatrix} \theta_1^e \\ \theta_2^e \end{bmatrix} + \begin{bmatrix} -c_3\dfrac{EI_1^e}{l^2} & c_4\dfrac{EI_2^e}{l^2} \\ c_4\dfrac{EI_1^e}{l^2} & -c_3\dfrac{EI_2^e}{l^2} \end{bmatrix} \begin{bmatrix} w_1^e \\ w_2^e \end{bmatrix} \tag{28}$$

where the subscripts '1' and '2' of M, EI, θ, and w denote left and right end nodes of the element, respectively, and the superscript 'e' denotes the eth element. The coefficients are as follows:

$$c_1 = \frac{2l\left[2l - R\sin\left(\dfrac{2l}{R}\right)\right]}{2l^2 - R^2 + R^2\cos\left(\dfrac{2l}{R}\right)}, \qquad c_2 = -\frac{4l\left[l\sin\left(\dfrac{l}{R}\right) - R\sin\left(\dfrac{l}{R}\right)\right]}{2l^2 - R^2 + R^2\cos\left(\dfrac{2l}{R}\right)}$$

$$c_3 = \frac{4l^2\sin^2\left(\dfrac{l}{R}\right)}{2l^2 - R^2 + R^2\cos\left(\dfrac{2l}{R}\right)}, \quad \text{and} \quad c_4 = \frac{4l^3\sin\left(\dfrac{l}{R}\right)}{2l^2R - R^3 + R^3\cos\left(\dfrac{2l}{R}\right)} \tag{29}$$

Eq. (28) can be rewritten as:

$$\mathbf{M}^e = \mathbf{S}\mathbf{w}_r^e + \mathbf{T}\mathbf{w}_t^e \tag{30}$$

where, the 2×1 vector, $\mathbf{M}^e$, denotes the internal moments at the two end nodes. The 2×1 vectors, $\mathbf{w}_r^e$ and $\mathbf{w}_t^e$, represent typically un-measurable rotations and measurable radial deflections,

respectively. The 2 × 2 matrices, **S** and **T**, denote element stiffness matrices with rotational DOF and radial DOF, respectively. The rotational DOF, $\mathbf{w}_r^e$, can be obtained by a direct inversion of the matrix, **S**:

$$\mathbf{w}_r^e = \mathbf{S}^{-1}\mathbf{M}^e - \mathbf{S}^{-1}\mathbf{T}\mathbf{w}_t^e \tag{31}$$

The explicit expression for Eq. (31) is as follows:

$$\begin{bmatrix}\theta_1^e\\ \theta_2^e\end{bmatrix} = \begin{bmatrix} d_1\dfrac{l}{EI_1^e} & d_2\dfrac{l}{EI_2^e}\\ -d_2\dfrac{l}{EI_1^e} & -d_1\dfrac{l}{EI_2^e}\end{bmatrix}\begin{bmatrix}M_1^e\\ M_2^e\end{bmatrix} + \begin{bmatrix} d_3\dfrac{1}{l} & -d_4\dfrac{1}{l}\\ d_4\dfrac{1}{l} & -d_3\dfrac{1}{l}\end{bmatrix}\begin{bmatrix}w_1^e\\ w_2^e\end{bmatrix} \tag{32}$$

where the geometric coefficients are as follows:

$$d_1 = -\frac{R}{2l}\cot\left(\frac{l}{R}\right) + \frac{1}{2}\csc^2\left(\frac{l}{R}\right), \quad d_2 = \left(\frac{R}{2l} - \frac{1}{2}\cot\left(\frac{l}{R}\right)\right)\csc\left(\frac{l}{R}\right)$$

$$d_3 = \frac{l}{R}\cot\left(\frac{l}{R}\right), \quad \text{and} \quad d_4 = \frac{l}{R}\csc\left(\frac{l}{R}\right) \tag{33}$$

Note that Eq. (32) reduces to the elementary slope-deflection equation of the Euler-Bernoulli beam when the radius R approaches infinity or the length l approaches zero:

$$d_1 \to \frac{1}{3}, \quad d_2 \to \frac{1}{6}, \quad d_3 \to 1, \quad \text{and} \quad d_4 \to 1, \quad \text{if} \quad l \to 0 \quad \text{or} \quad R \to \infty \tag{34}$$

2.3 Flexural damage index equation

In this section, the flexural damage index equation is derived using the previously derived slope deflection equation. Consider the two adjacent elements, denoted by e and $e+1$, in a global coordinate system (Fig. 3). For instance, the end nodes of the eth element are denoted by $i-1$ and i. Using Eq. (32), the rotational DOF of the eth element at the ith node can be expressed in terms of the primary nodal variables.

$$\theta_2^e = -d_2\frac{M_{i-1}l}{EI_{i-1}} - d_1\frac{M_i l}{EI_i} + \frac{d_4 w_{i-1} - d_3 w_i}{l} \tag{35}$$

Similarly, the rotational DOF of the $e+1$th element at the ith node becomes:

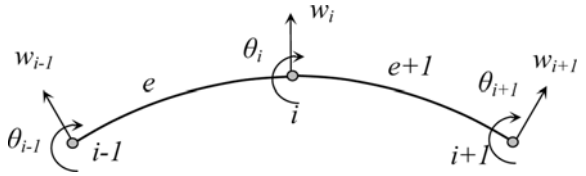

Fig. 3 Global coordinates of the curved elements

$$\theta_1^{e+1} = d_1\frac{M_i l}{EI_i} + d_2\frac{M_{i+1} l}{EI_{i+1}} + \frac{d_3 w_i - d_4 w_{i+1}}{l} \tag{36}$$

Note that the slopes of the two elements are identical at the *i*th node. Hence, a continuity condition gives rise to the following equation:

$$\theta_2^e = \theta_1^{e+1} \tag{37}$$

Substituting Eq. (35) and Eq. (36) into Eq. (37) yields:

$$d_2\frac{M_{i-1}}{EI_{i-1}} + 2d_1\frac{M_i}{EI_i} + d_2\frac{M_{i+1}}{EI_{i+1}} = \frac{d_4 w_{i-1} - 2d_3 w_i + d_4 w_{i+1}}{l^2} \tag{38}$$

If the curved beam is damaged, the analogous form of Eq. (38) can be described as:

$$d_2\frac{M_{i-1}^*}{EI_{i-1}^*} + 2d_1\frac{M_i^*}{EI_i^*} + d_2\frac{M_{i+1}^*}{EI_{i+1}^*} = \frac{d_4 w_{i-1}^* - 2d_3 w_i^* + d_4 w_{i+1}^*}{l^2} \tag{39}$$

where the superscript, '*', denotes the damaged states.

The small deflection theory requires that the change in shape of a structure due to a force must not affect the line of action of the applied load (Timoshenko and Gere 1963). Based on this approximation, the initial configuration can be used for the computation of internal forces caused by the applied loads. It is further assumed that the additional change in beam shape caused by a small damage event under a given loading condition may not affect the applied loads' line of action. The application of such a small damage assumption, $M_i^* \approx M_i$, into Eq. (39) yields:

$$d_2\frac{M_{i-1}}{EI_{i-1}^*} + 2d_1\frac{M_i}{EI_i^*} + d_2\frac{M_{i+1}}{EI_{i+1}^*} = \frac{d_4 w_{i-1}^* - 2d_3 w_i^* + d_4 w_{i+1}^*}{l^2} \tag{40}$$

With the aid of Eq. (15) and Eq. (6b), the moment-curvature relationship at the *i*th node can be obtained by:

$$M_i = EI_i\chi_i \tag{41}$$

where χ_i denotes the curvature of an intact structure. Substituting Eq. (41) into Eq. (40) yields the Flexural Damage Index Equation (FDIE) for the curved thin beam:

$$d_2\chi_{i-1}\beta_{i-1} + 2d_1\chi_i\beta_i + d_2\chi_{i+1}\beta_{i+1} = \gamma_i^* \tag{42}$$

in which

$$\beta_i = \frac{EI_i}{EI_i^*} \tag{43}$$

$$\chi_i = \frac{w_i}{R} + \frac{w_{i-1} - 2w_i + w_{i+1}}{l^2} \tag{44}$$

$$\gamma_i^* = \frac{d_4 w_{i-1}^* - 2d_3 w_i^* + d_4 w_{i+1}^*}{l^2} \tag{45}$$

where β_i is a damage index that is a ratio of the undamaged flexural rigidity to the damaged flexural rigidity at the ith node. For instance, if the severity of damage at the ith node is 10% ($EI_i^* = 0.9EI_i$), the damage index β_i becomes 1.1111. Similarly, the damage index will be a unity at the undamaged location. χ_i and γ_i^* can be numerically estimated at the ith node using the jth modal flexibility vector of an undamaged structure and a damaged structure, respectively. Hence, the unknowns that are supposed to be identified in Eq. (42) are the damage index, β_i, and the others, χ_i and γ_i^*, are the measured constants at the ith node. When the radius R approaches infinity or the length of the element l goes to zero, Eq. (42) approaches the linear FDIE for a beam (Kim *et al.* 2002):

$$\kappa_{i-1}\beta_{i-1} + 4\kappa_i\beta_i + \kappa_{i+1}\beta_{i+1} = 6\kappa_i^* \tag{46}$$

where $\kappa_i = d^2w_i/ds^2$ denotes the undamaged curvature of Euler-Bernoulli beam at the ith node. Note that χ_i and γ_i^* approach the curvature profile of undamaged and damaged structure, respectively, when the radius R approaches infinity.

The estimation of the curvature profile is necessary when using the dynamically measured jth modal flexibility vector. Since a coarse sensor interval is typically employed in practice, a cubic *Spline* interpolation of the jth modal flexibility vector is considered to be a prerequisite. Suppose that the jth modal flexibility vectors are measured at the N_0 nodes and they are interpolated at the N nodes for a circular arch with simply supported end conditions. Then the explicit expression of the FDIE of Eq. (42) for such a structure is as follows;

$$\begin{bmatrix} 2d_1\chi_2 & d_2\chi_3 & 0 & 0 & 0 & 0 & 0 \\ d_2\chi_2 & 2d_1\chi_3 & d_2\chi_4 & 0 & 0 & 0 & 0 \\ 0 & d_2\chi_3 & 2d_1\chi_4 & d_2\chi_5 & 0 & 0 & 0 \\ \vdots & \vdots & \ddots & \ddots & \ddots & \vdots & \vdots \\ 0 & 0 & 0 & d_2\chi_{N-4} & 2d_1\chi_{N-3} & d_2\chi_{N-2} & 0 \\ 0 & 0 & 0 & 0 & d_2\chi_{N-3} & 2d_1\chi_{N-2} & d_2\chi_{N-1} \\ 0 & 0 & 0 & 0 & 0 & d_2\chi_{N-2} & 2d_1\chi_{N-1} \end{bmatrix} \begin{bmatrix} \beta_2 \\ \beta_3 \\ \beta_4 \\ \vdots \\ \beta_{N-3} \\ \beta_{N-2} \\ \beta_{N-1} \end{bmatrix} = \begin{bmatrix} \gamma_2^* \\ \gamma_3^* \\ \gamma_4^* \\ \vdots \\ \gamma_{N-3}^* \\ \gamma_{N-2}^* \\ \gamma_{N-1}^* \end{bmatrix} \tag{47}$$

where the damage index at the two end nodes can be set as a unity ($\beta_1 = \beta_N = 1$), because the curvature is equal to zero ($\chi_1 = \chi_N = 0$) at the simply supported ends and the damage index can be arbitrary. The set of the FDIE in Eq. (47) is also valid for the j+1th modal flexibility vector. Hence, a sufficient number of equations at the interpolated nodes, denoted by m, can be constructed. The total possible number of equations is $(N-2)\times(N_0-2)$. However, the number of unknowns is only $N-2$, denoted by n. Therefore, a set of FDIEs results in an over-determined system of linear equations:

$$\Lambda\beta = \gamma^* \tag{48}$$

where the $n \times 1$ vector, β, denotes the unknown damage index vector; the $m \times 1$ vector, γ^*, denotes a damaged curvature of the curved beam; and the $m \times n$ matrix, Λ, represents the curvature set of

the undamaged curved beam. An efficient *pseudo-inverse* solution of Eq. (48) that satisfies all the Moore-Penrose conditions (Golub and Van Loan 1996) is

$$\beta = \mathbf{Y}\Omega^{-1}\mathbf{Y}^{T}\Lambda^{T}\gamma^{*} \tag{49}$$

in which

$$\Lambda^{T}\Lambda = \mathbf{Y}\Omega\mathbf{Y}^{T} \tag{50}$$

where the $n \times m$ matrix $\mathbf{Y}$ and the $m \times m$ matrix Ω are sets of singular vectors and singular values of a $m \times m$ symmetric matrix $\Lambda^{T}\Lambda$, respectively.

In theory, one set of the jth modal flexibility vector in Eq. (47) may predict the exact solution if the rank of Λ is full. However, the over-determined equation is inherently recommended because of measurement noise in the modal flexibility. For example, the reciprocal theorem of the jth modal flexibility vector in Eq. (3), $w_{kj} = w_{jk}$, is achievable. However, w_{kj} and w_{jk} are not exactly identical in the dynamically measured modal flexibility. Small errors in measurements of modal flexibility always exist. If there is no noise in the mode shapes, then only one set of the FDIE is needed to obtain an accurate solution.

In principle, two sets of linear algebraic equations have the identical solutions if their singular values are the same. Note that the singular value decomposition of the $m \times n$ $\Lambda^{T}\Lambda$ matrix, instead of the $m \times n$ matrix Λ, is performed in Eq. (50). Since the maximum possible rank of the matrix Λ is only n, the large number of equations, m, is unnecessary if the number of nonzero singular values in the matrix Λ becomes n. In practice, a few numbers of modal flexibility are enough to reach maximum rank n. In addition, the column choice in the modal flexibility matrix is arbitrary. The resulting solutions are insignificantly altered by column choice in the modal flexibility matrix if the rank of Λ is full.

The derived FDIE for a curved beam is seen to have the following four features. First, localized inspection may be feasible because no boundary conditions are imposed in the previous derivation of the FDIE. Second, the solution at the singular point may be achieved because the other adjacent nodes may not be singular and they are correlated through the FDIE. Third, a representative solution can be obtained using more than one mode because modal flexibility inherently provides a rational way to combine multi-modes. Finally, inspecting the resulting solution of the FDIE yields the location and the absolute severity of damage simultaneously.

3. Numerical study

In order to examine the performance of the derived FDIE for a circular arch, the simply supported circular arch in Fig. 4 is considered. The structural properties of the simulated arch consist of Young's modulus of 200 GPa, density of 7870 kg, radius of 1.0 m, a subtended angle (central angle) of $\pi/3$, and uniform rectangular cross sections of 0.04 m wide and 0.02 m high. This model is similar to that studied by Cerri and Ruta (2004). Damage is simulated by reducing the flexural rigidity, EI, in the damaged region indicated by the gray area in Fig. 4. The severity of damage is simulated by a 10% uniform reduction of flexural rigidity. Thus the exact damage index that is supposed to be predicted is 1.1111 in the damaged region. To measure flexural mode shapes, the 21 sensors ($N_0 = 21$) are placed with a uniform interval of $\pi/30$. Assuming that only the radial degrees

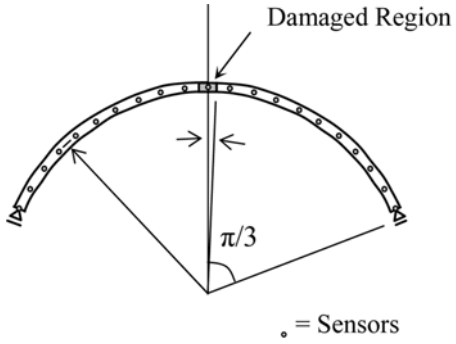

Fig. 4 Damage detection scenario of a simply supported circular arch

of freedom are measured at each sensor, the first three frequencies and displacement-normalized mode shapes are extracted for the structure before and after a small damage event. To numerically extract such eigenpairs, the 80 linear beam elements are used. The measured natural frequencies and mode shapes of the intact structure are shown in Fig. 5. Note that the changes in the first three natural frequencies are only 0.027%, 0.4026%, and 0.0112%, respectively. The changes in the first and third modes are significantly small because the location of damage is around the nodal point of the corresponding mode shapes. After a cubic *Spline* interpolation at the 201 nodes (N = 201), the trapezoidal line integration rule is used to obtain the flexural modal mass for each mode. Based on Eq. (4), the changes in modal mass are 0.0151%, 0.9706%, and 0.1580% for the three flexural modes, respectively.

Using the estimated modal mass, three sets of 21 × 1 modal flexibility vectors, due to a unit load at $\alpha = 2\pi/5$, $\pi/3$, and $\pi/2$, are computed by Eq. (1). Recall that choice of the location of a unit is arbitrary. Using the cubic *Spline* interpolation with a 0.0866 m uniform interval, the set of modal flexibility vectors is interpolated at N = 201 nodes. Then, the damaged and undamaged curvatures of three sets of modal flexibility vector are approximated by Eqs. (44) and (45), respectively. Here,

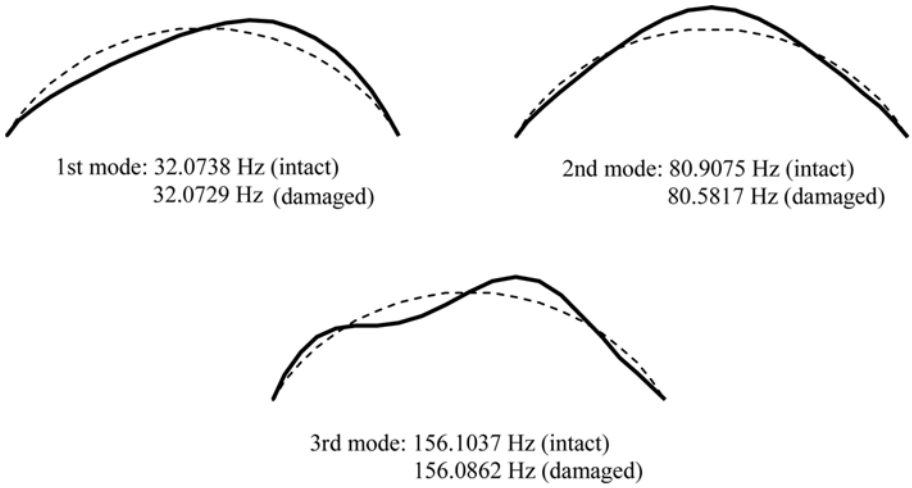

Fig. 5 Modal parameters of finite element model

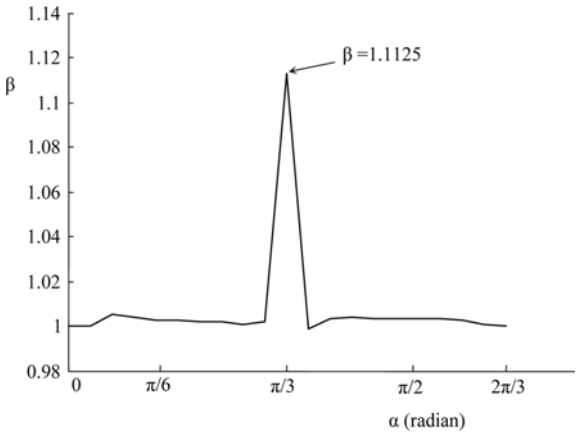

Fig. 6 Estimated damage index by the FDIE

the geometric coefficients, d_1, d_3, d_3 and d_4 in Eq. (33) are 0.3333367, 0.1666675, 0.999975, and 1.000012, respectively. Note that these values are close to those of a linear thin beam. To identify unknown damage indices at the 201 nodes, the 597 (199 × 3) coupled FDIEs are constructed with the aid of Eq. (42). The next step involves solving the over-determined equation using the pseudo-inverse technique in Eq. (49). Note that the matrix size of the required SVD process, $\Lambda^T\Lambda$, in Eq. (50) is only 199 × 199 instead of 597 × 199. The estimated damage indices at the only sensor locations are shown in Fig. 6.

The location of damage is clearly identified. Furthermore, the estimated severity of damage at the damaged location is $\beta = 1.1125$. Thus it can be interpreted that the flexural rigidity is reduced to 89.89% (1/1.1125) at the damaged region. Note that the percentile error of this severity estimation is only –0.12%. When the same solution procedures are applied with the geometric coefficients for a linear beam in Eq. (34), the percentile error of the severity estimation becomes 0.26% at the damaged region. This result indicates that the linear FDIE can also be used for damage detection of arches, but the proposed curved FDIE guarantees more accuracy.

For the purpose of comparative study, the DI method of Stubbs *et al.* (1995) and the MSC method of Pandey *et al.* (1999) are applied to the simulated arch with the same damage scenario. For the DI method, the damage index of the jth beam element β_j is defined as

$$\beta_j = \sum_{i=1}^{r} \frac{\left(\int_{L_j} (\bar{\phi}_i'')^2 dx + \int_0^L (\bar{\phi}_i'')^2 dx\right) \int_0^L (\phi_i'')^2 dx}{\left(\int_{L_j} (\phi_i'')^2 dx + \int_0^L (\phi_i'')^2\right) \int_0^L (\bar{\phi}_i'')^2 dx} \tag{51}$$

where L denotes total length of the beam; L_j denotes the length of the jth element; r denotes the number of modes considered; ϕ_i'' denotes the ith curvature mode shape of the undamaged states; and $\bar{\phi}_i''$ denotes the ith curvature mode shape after the damage event. Then, the normalized damage indicator Z_j of the jth element is defined as

$$Z_j = \frac{\beta_j - \mu_{\beta_j}}{\sigma_{\beta_j}} \tag{52}$$

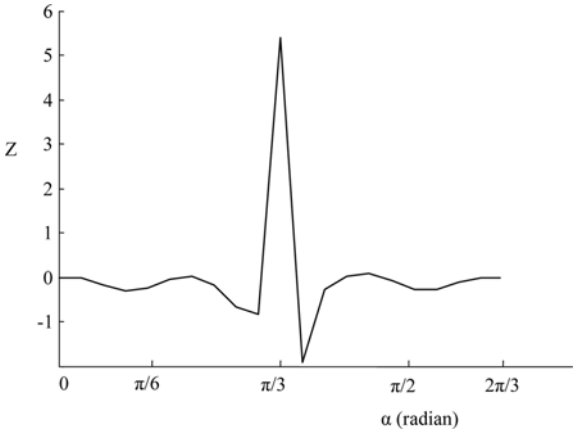

Fig. 7 Normalized damage index by the DI method

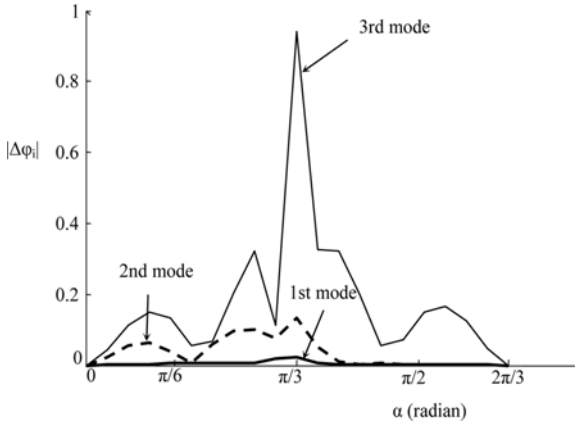

Fig. 8 Absolute curvature differences by the MSC method

where μ_{β_j} and σ_{β_j} denote the arithmetic mean and standard deviation of β_j, respectively. For each of the mode shapes, the finite difference formula is applied to compute the curvature mode shape after the cubic *Spline* interpolation at the 201 nodes. Next, the numerical integrations with the trapezoidal rule are performed. The estimated damage indices for the three modes are shown in Fig. 7. The clear peak near the simulated damage region is identified. To estimate the severity of damage, a sensitivity-updating algorithm, which is a model-based approach, can further be applied (Stubbs and Kim 1996). However, unlike the proposed FDIE method, the quantitative severity estimation of damage is not attainable by directly inspecting the normalized damage indices. For the MSC method, the absolute differences of each mode shape curvature are compared in Fig. 8. No refined interpolation processes are applied. Note that a clear peak in the second mode is distinguishable from the others at the damaged region. This is because the simulated damage locates at the nodal point of the first and third mode shape. This result clearly shows the mode selection problem previously discussed. It is seen that the MSC method has only succeeded in locating damage. However, the quantitative estimation of damage severity could not be obtained as with the DI method.

The applicability of the proposed method, under real conditions of measurement, is investigated by considering a type of noise. Possible noises involved in modal parameter measurements may be classified as two types. One is for sensor tilt caused by inaccurate installation. The other is for random signal noise in the measured time series. The problem associated with accurate modal parameter extraction in severe random noise conditions is out of the scope of this study. Usually, the statistic manipulation through the repeated modal tests and analyses with the proper selection of sensor sensitivity provides a set of averaged clean mode shapes that has small standard deviation and variance. Only noise caused by tilt is considered here because true modal parameters in such noise conditions may not be recovered. Assume that accelerometers cannot be installed exactly perpendicular to the surface of the arch, and their biased angles are randomly distributed from -5^o to 5^o in tangential directions. Such noise is numerically considered by taking the cosine function of random angles within such a range. Also assume that the sensors are not moved before and after a small damage event. Using mode shapes with such simulated noise, the same FDIE solution procedures are performed. The damage indices identified at the sensor locations are shown in Fig. 9.

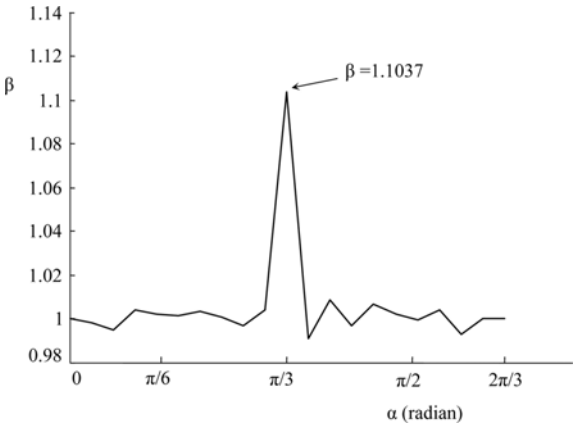

Fig. 9 Estimated damage index with tilt noise

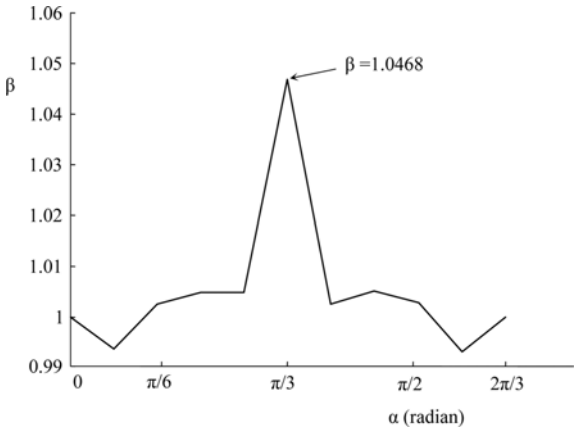

Fig. 10 Estimated damage index with a larger sensor spacing

Damage localization is shown to be successful, but the error of the severity estimation at the damaged region increases to 0.664%.

To investigate the effect of sensor spacing, a coarser sensor interval is examined. The eleven sensors are placed with a uniform spacing of $\pi/15$ from $\alpha = 0$ to $\alpha = 2\pi/3$. Identical FDIE solution procedures are repeated for the same single damage scenario. The predicted damage indices are shown in Fig. 10. Although the localization of damage is successful, the error in the severity estimation at the damaged region increases to 5.78%; this result may not be satisfactory for certain applications. To resolve this deficiency, the eleven sensors can be moved to the damaged region using *a priori* knowledge of the predicted damage locations shown in Fig. 10. The sensors are placed from $\alpha = 31\pi/120$ to $\alpha = 51\pi/120$ with a uniform sensor spacing of $\pi/60$. The predicted damage indices, attained using the identical solution procedures for only three modes, are shown in Fig. 11. The error of severity estimation is reduced to –2.07% at the peak. This result yields two observations: first, the proposed method is capable of local inspection even though mode shapes are

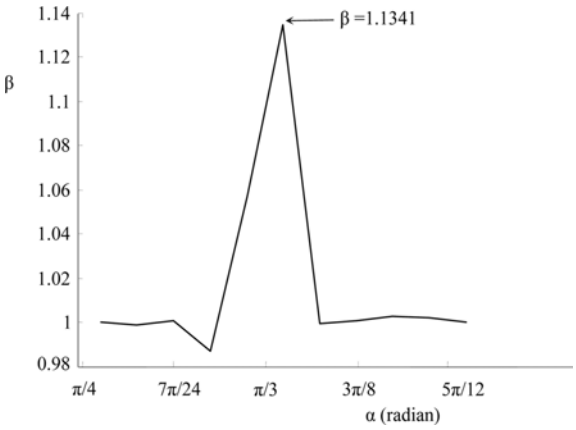

Fig. 11 Estimated damage index for local inspection

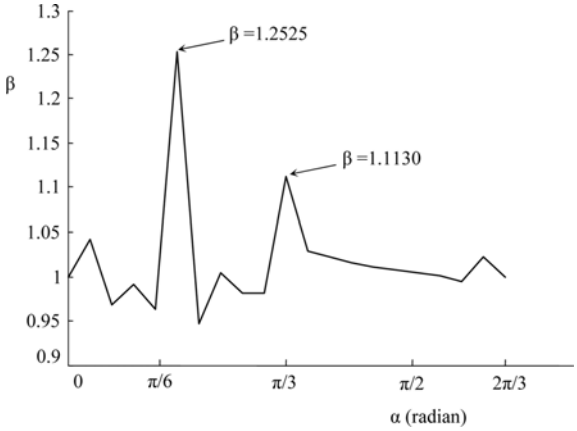

Fig. 12 Estimated damage index for multiple damage

either spatially or temporally incomplete; second, the accuracy of damage severity estimation relies on the sensor spacing even though the localization of damage is successful.

To investigate the performance of the proposed method for a multiple damage scenario, an additional damage region is considered. The additional damage region is intentionally placed near the nodal points of the second and third mode shape. The exact location of the additional damage lies between $\alpha = 3\pi/20$ and $\alpha = \pi/6$. The exact severity of damage is $\beta = 1.25$ (1/0.8) because of a 20% uniform reduction in flexural rigidity. The first three natural frequencies with two damaged regions are 31.7827 Hz, 80.2131 Hz, and 156.0527 Hz, respectively. The same 21 sensor locations are used, and the identical FDIE solution procedures are conducted. The identified damage indices are depicted in Fig. 12. Two clear peaks are identified at the two simulated damaged regions. The errors of damage severity estimation are –0.1991% and –0.1734% at $\alpha = \pi/6$ and $\alpha = \pi/3$, respectively. This result indicates that the proposed method is capable of evaluating damage in multiple locations.

4. Conclusions

The objective of this study is to introduce a newly developed vibration-based NDE method for a selected class of structures that attempts to resolve some deficiencies associated with earlier works. To meet this goal, the fundamental concept of the jth modal flexibility vector is summarized, and the slope-deflection equations for a curved beam have been derived. Next, the FDIE are achieved with a small damage assumption. Then, an efficient solution technique has been introduced to solve the set of previously derived FDIE for the considered structure. Finally, various aspects of the performance of the proposed method have been numerically evaluated.

Based on the results of the numerical experiments, the following five findings can be stated. First, the mode selection and singularity problems of earlier attempts are not an obstacle in the proposed approach. Second, the proposed method provides not only the location of damage, but also the severity of damage through direct inspection of the estimated damage indices. Third, the proposed approach makes localized detail inspection with incomplete mode shapes possible. Fourth, identification of structural damage in multiple locations is also feasible. Finally, the sensor interval significantly affects the accuracy of the damage severity estimation. This may be due to the interpolated error of curvature measured between two sensor nodes. This deficiency requires that mode shapes be measured with a refined sensor interval.

Acknowledgements

This work is financially supported by the Korea Ministry of Construction and Transportation (MOCT) (05 Base Construction D04-01).

References

Berman, A. and Flannelly, W.G. (1971), "Theory of incomplete models of dynamic structures", *AIAA J.*, **9**(8), 1481-1487.

Cawley, P. and Adams, A.D. (1979), "The location of defects in structures from measurements of natural frequencies", *J. of Strain Analysis*, **14**(2), 49-57.
Cerri, M.N. and Ruta, G.C. (2004), "Detection of localized damage in plane circular arches by frequency data", *J. Sound Vib.*, **270**, 39-59.
Chen, Y. and Swamidas, A.S.J. (1994), "Dynamic characteristic and modal parameters of a plate with a small crowing surface crack", *Proc. 12th IMAC,* Honolulu, Hawaii, **2**, 1155-1161.
Choi, S. and Stubbs, N. (1997), "Nondestructive damage detection algorithms for 2D plates Smart Structures and Materials: Smart System for Bridges, Structures, and Highways SPIE", *Proc.* No. 3043, 193-204.
Cornwell, P., Doebling, S.W. and Farrar, C.R. (1999), "Application of the strain energy damage detection method to plate-like structures", *J. Sound Vib.,* **224**(2), 359-374.
Doebling, S.W., Peterson, L.D. and Alvin, K.F. (1996), "Estimation of reciprocal residual flexibility from experimental modal data", *AIAA J.,* **34**(8), 1678-1685.
Ewins, D.J. (2000), *Modal Testing: Theory, Practice and Application* (2nd Ed.), Research Studies Press Ltd., Hertfordshire, England.
Farrar, C.R. and Jauregui, D. (1998), "Comparative study of damage identification algorithms applied to a bridge: I. Experiment", *Smart Materials and Structures,* **7**, 704-719.
Farrar, C.R., Cornwell, P.J., Doebling, S.W. and Prime, M.B. (2000), "Structural health monitoring studies of the Alamosa canyon and I-40 bridges", Report No., LA-13635-MS, Los Alamos: Los Alamos National Laboratory.
Golub, G.H. and Van Loan, C.F. (1996), *Matrix Computations*. 3rd Ed., Baltimore, The Johns Hopkins University Press.
Kim, B.H., Stubbs, N. and Sikorsky, C. (2002), "Local damage detection using modal data", *Proc. 20th IMAC,* Los Angzeles, CA, 435-441.
Mottershead, J.E. and Friswell, M.I. (1993), "Model updating in structural dynamics: A survey", *J. Sound Vib.,* **167**(2), 347-375.
Ndambi, J.M., Vantomme, J. and Harri, K. (2002), "Damage assessment in reinforced concrete beams using eigenfrequencies and mode shape derivatives", *Eng. Struct.,* **24**, 501-515.
Pandey, A.K., Biswas, M. and Samman, M.M. (1999), "Damage detection from changes in curvature mode shapes", *J. Sound Vib.*, **145**(2), 321-332.
Salawu, O.S. (1997), "Detection of structural damage through changes in frequency: A review", *Eng. Sci.*, **19**(9), 718-723.
Salawu, O.S. and Williams, C. (1994), "Damage location using vibration mode shapes", *Proc. 12th IMAC*, Honolulu, Hawaii, **1**, 933-939.
Srinivasan, M.G. and Kot, C.A. (1998), "Damage index algorithm for a circular cylindrical shell", *J. Sound Vib.,* **215**(3), 587-591.
Stubbs, N. (1985), "A general theory of non-destructive damage detection in structures", In: Leipholz HHH, editors. *Structural Control: Proc. of the 2nd Int. Symposium on Structural Control*, Netherlands, Martinus Nijhoff Publishers, 694-713.
Stubbs, N. and Kim, J.T. (1996), "Damage localization in structures without baseline modal parameters", *AIAA J.*, **34**(8), 1644-1649.
Stubbs, N., Kim, J.T. and Farrar, C.R. (1995), "Field verification of a nondestructive damage localization and severity estimation algorithm', *Proc. 13th IMAC*, Nashville, Tennessee, **1**, 210-218.
Timoshenko, S. and Gere, J.M. (1963), *Theory of Elastic Stability*. 2nd Ed. New York: McGraw-Hill, Inc..
Wahab, M.M.A. and Roeck, G.D. (1999), "Damage detection in bridges using modal curvature: Application to a real damage scenario", *J. Sound Vib.*, **226**(2), 217-235.